Advanced Materials Research *Online: 2014-05-23*
ISSN: 1662-8985, Vols. 926-930, pp 218-221
doi:10.4028/www.scientific.net/AMR.926-930.218

Research the Effect of Forced Flow on Dendritic Growth with Adaptive Finite Element Method

Changsheng Zhu[1, a,*], Peng Lei[1, b] and Rongzhen Xiao[2, c]

[1]College of Computer and Communication, Lanzhou University of Technology, Lanzhou 730050, China;

[2]State Key Laboratory of New Non-ferrous Metal Materials, Lanzhou University of Technology, Lanzhou 730050, China

[a]867320505@qq.com, [b]lp2011_lucky@sina.com, [c]119235627@qq.com

Keywords: Phase-field model, forced flow, dendritic growth, adaptive finite element.

Abstract. Phase-field model coupled with flow field is solved by the adaptive finite element method. The simulation results show that the forced flow can induce side-branches though there is no thermal noise. When the flow velocity is low, the symmetry of dendrite morphology is slightly influenced by forced flow. With the increase of flow velocity, the symmetry of dendrite morphology is collapsed completely.

Introduction

Dendrite is a form of most casts and microstructure during solidification. The dendrite growth is a complex physical process, and it is influenced by transportation of heat, mass and momentum[1]. In recent years, phase field model provides a very convenient and effective method for study of dendrite growth[2,3,4]. It is a good tool to simulate the evolution mechanism of the complex interface during the process of solidification. However, the adaptive finite element method based on non-uniform grid is more efficient and less amount of calculation than the method based on uniform grid when solving phase-field model[5]. Therefore, the adaptive finite element algorithm [6] and the functional library AFEPack[7] are employed to solve phase-field model in this paper. The dendritic growth of nickel is simulated quantitatively, and the effect of flow forced flow on dendrite morphology is investigated.

Simulation Model

Phase-field model. The equations of phase-field model should be transformed into the corresponding week forms before employing the adaptive finite element method, and the trial functions $g(x, y)$ and $h(x, y)$ are introduced. According to Green's theorem and the formula integration by parts, the phase-field model coupled with flow and the form of thermal noise are given by:

$$\begin{aligned}&\int_\Omega \frac{\varepsilon^2}{m}\frac{\varphi^{t+\Delta t}}{\Delta t} g d\Omega + \int_\Omega \varepsilon^2\eta(\theta)^2 \nabla g\cdot\nabla\varphi d\Omega - \int_\Omega \varepsilon^2\eta(\theta)\eta'(\theta)\frac{\partial g}{\partial x}\frac{\partial \varphi^{t+\Delta t}}{\partial y} d\Omega \\ &+\int_\Omega \varepsilon^2\eta(\theta)\eta'(\theta)\frac{\partial g}{\partial y}\frac{\partial \varphi^{t+\Delta t}}{\partial x} d\Omega = \int_\Omega \frac{\varepsilon^2}{m}\frac{\varphi^t}{\Delta t} g d\Omega \\ &+\int_\Omega \varphi^t(1-\varphi^t)[\varphi^t - \frac{1}{2} + 30\varepsilon\alpha Su\varphi^t(1-\varphi^t)] g d\Omega + \int_\Gamma \varepsilon^2\eta(\theta)^2 \frac{\partial \varphi^t}{\partial n} g ds\end{aligned} \tag{1}$$

$$\frac{\varepsilon^2}{m}\frac{\partial\varphi}{\partial t} \to \frac{\varepsilon^2}{m}\frac{\partial\varphi}{\partial t} + 16\varphi^2(1-\varphi)^2 R\mathrm{f} \times 30\varepsilon\alpha Su\varphi^2(1-\varphi)^2 \tag{2}$$

$$\int_\Omega \frac{u^{t+\Delta t}}{\Delta t} h d\Omega + \int_\Omega \nabla u\cdot\nabla h d\Omega = \int_\Omega \frac{u^t}{\Delta t} h d\Omega - \int_\Omega \frac{p'(\varphi)}{S}\frac{\partial\varphi}{\partial t} h d\Omega - \int_\Omega F(\varphi) V\cdot\nabla u h d\Omega + \int_\Gamma \frac{\partial u}{\partial n} h ds \tag{3}$$

The dimensionless temperature $u = (T - T_m)/(T_m - T_0)$, where T_m is the melting temperature, and T_0 is the initial temperature of system. Dimensionless supercooling degree $S = C_p(T_m - T_0)/L_m$,

where C_p is specific heat at constant pressure, and L_m is the latent heat. The interfacial migration coefficient $m = \mu\sigma T_m / (\kappa L_m)$, where μ denotes interface migration rate, σ represents interface energy . The anisotropic factor $\eta(\theta) = 1 + \gamma\cos[M(\theta)]$. In Eq. (3), $F(\varphi)$ is given by:

$$F(\varphi) = \begin{cases} 0 & \varphi < 0.7 \\ \varphi & \varphi \geq 0.7 \end{cases} \tag{4}$$

The conservation equations of mass and momentum. The conservation equations of mass and momentum are given by:

$$F(\varphi)\nabla \cdot V = 0 \tag{5}$$

$$F(\varphi)\frac{\partial V}{\partial t} + F(\varphi)(V \cdot \nabla)V = \frac{1}{\mathrm{Re}}\nabla^2 V - F(\varphi)\nabla p \tag{6}$$

Where p is pressure, and Re denotes Reynolds number.

The mass and momentum equations are solved numerically by using the fractional-step projection algorithm[8]. To guarantee unconditional stability and avoid any restriction on the time step, the advection term $(V \cdot \nabla)V$ in Eq.(6) is replaced by its skew-symmetric for $(V \cdot \nabla)V + 1/2(\nabla \cdot V)V$, and the advection–diffusion step is given by:

Where $\overline{V}^{k+1}$ stands for intermediate velocity value, and V^{k+1} denotes divergence-free velocity field.

The computational properties of nickel

The materials properties of phase-field model are shown in Table 1.

Table 1 The computational properties of nickel

Parameters	Values	Parameters	Values
T_m(K)	1728	S	0.65
L_m(J·cm^{-3})	2350	θ	0
C_p(J·K^{-1}·cm^{-3})	5.42	ε	0.002
κ(cm^2·s^{-1})	0.155	M	4
μ(cm·K^{-1}·s^{-1})	285	$\Delta x = \Delta y$	0.04
σ(J·cm^{-2})	3.7×10^{-5}	γ	0.05
l(cm)	2.1×10^{-4}	Δt	6.0×10^{-6}

Initial condition and boundary condition

An initial nuclear of the radius r0 can be defined as:

$$\begin{cases} \varphi = 0 \quad u = 0 \quad V_x = 0 \quad V_y = 0 \quad p = 0 \quad x^2 + y^2 \leq r_0^2 \\ \varphi = 1 \quad u = -1 \quad V_x = 0 \quad V_y = U_0 \quad p = 0 \quad x^2 + y^2 > r_0^2 \end{cases} \tag{7}$$

Where V_x, V_y are the flow velocities along x and y respectively. Supercooled melt enters the domain from the top boundary with a uniform velocity U0 and exits from the bottom boundary. The Zero-Neumann boundary conditions are imposed at the boundaries of the computational domain for phase field and thermal field, while the mass and momentum equations are employed no-slip boundary conditions.

Results and Discussion

Fig.1(a) and Fig.1(b) show the dendrite morphology and temperature field distribution at $t = 6500\Delta t$. The thermal noise strength is f=0. The coefficient of viscosity is ν=0.005443(m^{2}s^{-1}), and the initial velocity is $U_0 d_0 / \kappa$=0.003. It can be seen that, the side-branches appear in upstream region without thermal noise, and the side-branches in upstream region are more developed than they are in downstream region, as shown in Fig.1(a). In downstream region, temperature gradient and the actual

undercooling are low due to forced flow, thus the growth of the dendrite gradually is restrained. In addition, thermal diffusion layer becomes thicker in downstream region, which prevents the release of the latent heat, as shown in Fig.1(b). Therefore, disturbance of interface is restrained, and fewer sides-branches appear in downstream region.

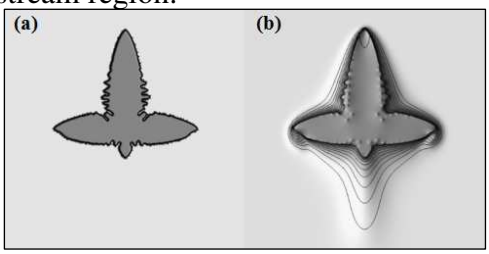

Fig.1 The phase-field dendrite morphology and corresponding temperature field distribution with flow at $t = 6500\Delta t$

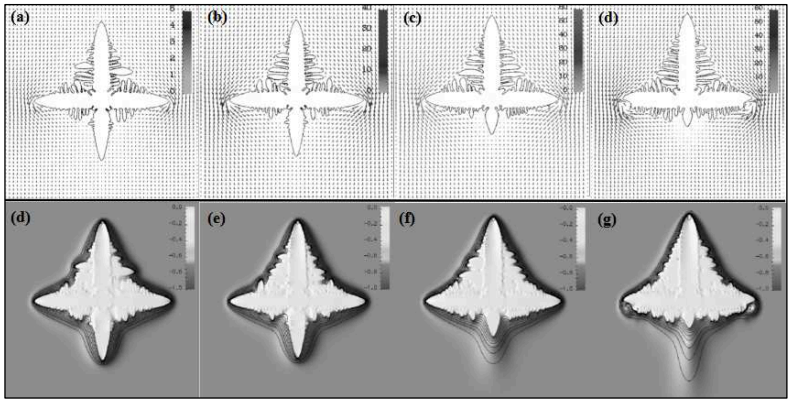

Fig. 2 The flow field and thermal distribution under different flow velocities at $t = 6900\Delta t$, where (a)(d)U0=0.068×10-3; (b)(e) U0=0.0025 ; (c)(f) U0=0.0026 ; (d)(g) U0=0.0036

The effect of forced flow on the growth velocities of upstream, normal and downstream dendrites is apparent. Fig.2 shows the dendrite shape at growth time of $t = 6500\Delta t$, where the initial flow velocities are U0=0, 0.0011, 0.0025, 0.0026 and 0.0036 respectively. It can be found that, when the flow velocity is less than 0.0026, the influence of forced flow on dendrite morphology is trivial, and the dendrite growth is mainly controlled by thermal diffusion. With the increase of flow velocity, the dendrite growth is controlled by the convection gradually.

Fig.3 shows the magnification of grids with dendritic growth corresponding to Fig.2 (a). It can be found that, the grids are refined near the solid-liquid interface and the grids are coarsened far away from the interface. So, number of nodes is reduced and the computational efficiency is improved when the adaptive finite element method is adopted to solve the phase-field model.

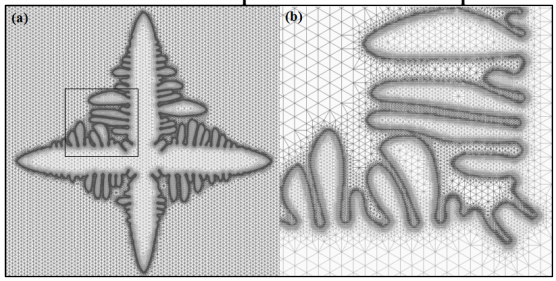

Fig. 3 The magnification of grids with dendritic growth

Conclusion

Although there is no thermal noise, side-branches can be induced by the effect of forced flow on dendritic growth. Side-branches in upstream region are more developed than they are in downstream region. When the flow velocity is low, the effect of forced flow on the dendrite morphology is trivial, but the symmetry of dendrite shape is collapsed obviously with increasing of the flow velocity. When

the adaptive finite element method is adopted to solve the phase-field model, the computational efficiency is improved greatly.

Acknowledgements

Foundation items: Project (Grant No. 51161011, No.11364024) supported by the National Natural Science Foundation of China.

Project (Grant No.1204GKCA065) supported by the Key Technology R&D Program of Gansu province ;Project(Grant No. 201210) supported by the Fundamental Research Funds for the Universities of Gansu province ; Project (Grant No. J201304) supported by the funds for Distinguished Young Scientists of Lanzhou University of Technology.

References

[1] X. Tong, C. Beckermann and A. Karma: Physical Review Letter E, Vol. 63 (2001) No. 6, p. 061601.1-061601.16.
[2] L. Yuan, D.P. LEE: Modeling and Simulation in Materials Science and Engineering, Vol. 18 (2010) No.5, p.055008-055020.
[3] Z.P. Wang, J.W. Wang, C.S. Zhu, L. Feng and R.Z. Xiao: Transactions of Nonferrous Metals Society of China, Vol. 21 (2011) No.3, p.612-617.
[4] J.W. Wang, Z.P. Wang, Y. Lu, C.S. Zhu, L. Feng,R.Z. Xiao: Transactions of Nonferrous Metals Society of China, Vol. 22 (2012) No.2, p.391-397.
[5] Y. Chen, K.H. Kang and D.Z. Li:Acta physica sinica, Vol.58 (2009) No.1, p.390-397.
[6] R. Li: Journal of Computing, Vol.24 (2005) No.3, p.321-341.
[7] Information on http://circus.math.pku.edu.cn/AFEPack.
[8] J.L. Guermond, L. Quartapelle: International Journal for Numerical Methods in Fluids, Vol.26 (1998), p.1039-1053.